Egypt. J. Chem. **Vol. 65,** No. SI:13B pp. 903-918 (2022)

Egyptian Journal of Chemistry

http://ejchem.journals.ekb.eg/

Enhancement Adsorption of Copper and Zinc Contaminated Water Using Highly Efficient Graphene Oxide Modified with Acid-Activated Bentonite

Sabah S. Ibrahim [a], Yasser K. Abdel-Monem [b], Abdallah A. Hasan [b*]

[a] *National Water Research Center (NWRC), El Qanater El Khayria, Egypt*

[b] *Chemistry department, Faculty of science, Menuofia University,* Shebin El-Kom, *Egypt*

Abstract

The efficient sorbents for the heavy metal ions elimination from wastewater, like graphene and carbon nanotubes, are widely utilized in nanomaterials development. Clays (bentonite), activated carbon, metal oxides, and zeolites are commonly used as adsorbents in the heavy metals removal from solutions, such as Pb (II), Zn (II), Cd (II), Ni (II), as well as Cu (II). The graphene oxide (GO), in this study, was produced from graphite powder using a modified Hummer's technique, then altered by doping with acid-activated bentonite. SEM, EDAX, TEM, FTIR, and XRD characterized modified graphene oxide. The Cu(II) and Zinc (II) were adsorbed onto the modified GO using the simple batch-adsorption mode. pH values, initial concentration, adsorbent dosage, reaction temperature, and contact time were used to successfully vary the percentage of removed Zn(II) and Cu(II).

At pH 5.6 under the ambient conditions (according to the diagram of zero point charge), over 45 min adsorption time, and 0.5 g/L adsorbent dose, the highest removal efficiency of Cu(II) and Zn(II) were 99.75% and 99.79%.

The highest adsorption capacities of modified GO were 39.896 and 39.954 (mg/g) for Cu(II) and Zn(II), respectively, and the experimental values correlate well with the Langmuir isotherm.

Keywords: heavy metal ions, adsorption, modified graphene oxide, carbon nanotubes, activated carbon, immobilization, kinetic.

1. Introduction

Heavy metals treatment and removal from water and wastewater are vital for environmental and public health protection. Copper and zinc ions are hazardous pollutants in wastewater that are harmful to the environment and living organisms in large amounts. [1]. Chemical precipitation [4], adsorption [5], ion exchange [6], membrane filtration [7], and electrochemical treatment [8] have all been developed to remove heavy metal ions from wastewater [2,3]. Because of its low cost and great efficacy, sorption is the most extensively used and economically advantageous of these approaches [9].

For heavy metals wastewater treatment, sorbents such as activated carbon, bio-adsorbents, resins, and molecular sieves are commonly utilized [10].

GO is one of the best adsorbents for heavy metal ions removal that contains interactive oxygen functional groups, e.g., carboxyl groups, epoxides, ketones, and hydroxyl [11]. GO, which has a large surface area and many oxygen atoms, is a potential material for heavy metal removal. However, using graphene oxide as a heavy metal adsorbent directly is unfeasible [12]. Because of strong interplanar contacts, GO tends to accumulate in a layer-by-layer pattern, which is inconvenient for adsorbent regeneration [13]. In addition, GO is also unstable at high temperatures. Cu^{2+} ions induce the graphene oxide layers to form numerous aggregates in aqueous solutions, according to research [14].

Modifying GO or producing GO composite materials to improve GO stability is required for improved practical applications [15,16].

Furthermore, GO has a surface area of up to 2620 m^2/g (theoretical value) and can be produced from cheap natural graphite on a large scale [17]. Graphene oxide, a new type of carbon nanomaterial, has piqued researchers' attention in a variety of

*Corresponding author e-mail: 3bdallah.ahmed90@gmail.com.; (Abdallah A. Abdallah).

Receive Date: 06 August 2022, Revise Date: 26 August 2022, Accept Date: 29 August 2022

DOI: 10.21608/EJCHEM.2022.154776.6690

domains, including biology, wastewater treatment, and electronics [18]. By modifying the surface chemistry of a substance, modification can improve the chemical characteristics of materials by providing capabilities, functional groups, or additional features. Functionalization is attaching process nanoparticles or molecules to a material surface, which can be done chemically or by sorption. Only the presence of oxygen-containing functional groups allows for the functionalization or modification of graphene oxide surfaces [19]. Recent studies have shown that GO is ideal for the sorption of dyes and heavy metals and a good catalyst carrier because of its mechanical strength and huge surface area [20,21]. The adsorption capacity of graphene oxide for Cu(II) ions is 46,6 mg/g, which is greater than the capacities of activated carbon and carbon nanotubes, which are 4–5 mg/g and 28,5 mg/g, respectively[22]. Ren and his colleagues came to the same conclusion by comparing the adsorption capabilities of three carbon materials (graphene oxide, multi-walled carbon nanotubes, and activated carbon) during Cu (II) ion sorption [23].

Bentonite, as an aluminosilicate clay representative, is a great alternative for ensuring that the required.

Two silica tetrahedral sheets fused to one alumina octahedral sheet make up the two-dimensional (2D) layered structure of bentonite [24]. The surface charge of clay minerals induced by the isomorphous replacement of layers by cations of lower valence is balanced via exchangeable cations such as Na^+ and Ca^{2+} [24,25]. Because of its high cation exchange capacity, cheap cost, high stability, excellent adsorption efficiency, and ease of production, bentonite is widely applied in the field of adsorption and separation [26,27].

The acid activation of bentonite was done using HCl at concentrations ranging from 0.05M to 0.5M.

In general, when the acid concentration rises, the surface area of acid-activated bentonite increases until it reaches a maximum, after which it gradually decreases. To investigate the influence of temperature on the alteration of bentonite by acid activation, the reaction temperature for acid activation was varied between 30°C, 60°C, and 80°C. When the acid concentration increased to 0.1M HCl, sorption capacity and surface area of bentonite increased.

With increasing acid activation, the sorption capability and surface area gradually decreased [28,29].

As the period was kept constant at 3 hours, an increase in activation temperature induced a decrease in surface area and adsorption capacity. When compared to crude bentonite, the sorption capacity and surface area of AA bentonite increased by 65 percent and 18 percent, respectively. [30]. The bentonite surface area was observed to increase as the acid strength grew. Surface area increases at low concentrations due to cation exchange and the elimination of contaminants; yet, surface area decreases due to sampling decomposition and structural variations. Smectites decompose more quickly when temperature and acid concentration rise, increasing the bentonite surface area in the process [31].

Various analytical techniques such as SEM, EDAX, TEM, XRD, and FTIR were used to demonstrate changes in the Physico-chemical characteristics of adsorbent.

This paper aims to study the Copper and Zinc adsorption behavior on modified graphene oxide based on pH influence, equilibrium adsorption capacity, initial concentration of metals, temperature, contact time, sorbent dosage, and kinetic studies influence. The modified Hummer's process was used to generate graphene oxide, which was subsequently transformed to modified GO by doping acid-activated bentonite with HCl, demonstrating that modified bentonite had better adsorption qualities than natural bentonite. The differences in the Physico-chemical properties of the adsorbent were demonstrated using different analytical techniques such as TEM, SEM, EDAX, FTIR, and XRD.

2. Experimental:

2.1. Chemicals and equipments

Graphite powder (< 20 μm), Potassium permanganate, concentrated sulfuric acid (98%), hydrogen peroxide (30%), hydrochloric acid (38%), sodium nitrate, bentonite, Copper (II) Chloride Dihydrate, Zinc (II) Choloride (Dry) 97%. The chemicals used in the study from Sigma Aldrich. For preparation, dilution, and analytical purposes: deionized water was employed. Magnetic stirrer, ice bath, beaker, magnetic bead, rotary shaker, dropper, funnel, cylinder, conical flask, thermometer, oven, crucible, and pH meter.

2.2. GO Synthesis

GO was produced by several researchers using a modified Hummer's procedure [32], then characterized the material by SEM, XRD, and FTIR [33].

Briefly, take a beaker and set it up in an ice bath under stirring, firstly add 125 ml concentrated sulfuric acid very carefully, then add 5-gram graphite powder, subsequently, 2.5 grams of sodium nitrate is added to the mixture under stirring, in the next step after 30 minutes add 15-gram potassium permanganate very slowly by keeping temperature less than 20 degrees.

The mixture was stirred for 2 hours under these conditions. After that, add deionized water until the temperature increases to 100 degrees after further stirring for 15 minutes while maintaining the same temperature. We observe color changes to dark brown, indicating the formation of graphene oxide. Fig.1a. Again add 100 ml of deionized water to oxidize the graphite left. The mixture is quenched and diluted by pouring it into 1.5 liters of deionized water. Finally, add hydrogen peroxide to remove an excessive amount of potassium permanganate or to stop the reaction. Stir continuously for another 2 hours until the evolution of hydrogen bubbles stops. The mixture was filtered to obtain the solid product, and the residue was rinsed five times with 0.6 N HCl solution and then with distilled water until the pH was neutral. The acquired material was vacuum dried to produce a fine brown powder.

2.3. Bentonite acid activation

The acid to clay ratio fixed at 1:10. In a shaker flask, 100 ml of 0.1 M HCl solution of known concentration added to 10 g of raw bentonite. The temperature was controlled at 300°C by keeping the shake flask in the rotary shaker. The acidified product was then rinsed with deionized water more than once. Further washing reached a pH of 5, and the filtrate was free of Cl^- ions. Finally, dry in an oven at 60 - 80°C for 2 hours.

2.4. synthesis of modified GO (Doping or Immobilization with bentonite)

About 100 g of GO mixed with fine powder acid-activated bentonite (1-7g).

0.125 g of acid-activated bentonite was added to the graphene oxide obtained (12.5 g) with further stirring. Finally, the mixture was washed using deionized water until the filtrate became clear, then measured pH for the filtrate before drying to be neutral.

2.5. Characterization of modified GO

The crystal structure of modified GO confirmed by X-ray diffractometry (XRD) carried out using a (Bruker co, D8 advance, Cu target, 40 kV 40 mA, Wavelength 1.45A, Germany).

Fourier transfer infrared (FTIR) analysis of the samples was carried out by (Thermo Scientific Nicolet iS10 spectrometer) for examination of the spectra in the wavenumber range of 4000–400 cm^{-1}. The modified GO was successfully synthesized, and the bentonite layer was situated on the surface of the GO, according to spectral analysis.

The particle morphology was examined using scanning electron microscopy(SEM). (FESEM, Quanta FEG250, made in Netherland). Energy-dispersive X-ray spectroscopy (EDAX) for samples.

The structure morphologies of modified GO were analyzed by transmission electron microscopy (TEM). (HRTEM, Model. JEM2100, Jeol jem2100, Japan, 200KV,1.5x).

2.6. Adsorption procedure

In a batch approach of operation for contact duration (10–120 minutes), the influences of experimental parameters of different pH values (2–12) that were changed with 0.1 M HCl or NaOH solutions at 25°C, initial metal ion concentration (10–30 mg/L) on the removal of Zinc and Copper were explored. In these studies, known Zinc and Copper sample solutions were placed in a (50) mL glass conical flask and stirred at various reaction periods, pH values, absorbent dosages, temperatures, and initial metal ion concentrations. Subsequently, the adsorbent (modified GO) was removed from the solutions, after adsorption, by filtration using a funnel.

Copper and Zinc concentrations in the solution were determined using an (ICP) device. The measurements were conducted three times, with the average of the results. Eq (1) was used to calculate the adsorption capacity, Qe (mg/g), and Eq (2) was used to estimate the removal rate (percent):

$$Q_e = (C_o - C_e)\, x \frac{V}{m} \quad (1)$$

$$\text{Removal rate}(\%) = \left(\frac{C_o - C_e}{C_0}\right) x100 \quad (2)$$

Where the adsorbate volume is V, C_e and C_o are metal concentrations (mg/L) after and before adsorption, and the adsorbent weight (g) is m.

3. Results and Discussions

3.1. Characterization of adsorbents

3.1.1. SEM and EDAX analyses:

SEM images help understand the microscale surface morphology of the GO samples. To see if Cu(II) and Zn(II) were adsorbed by bentonite/GO, SEM and EDAX analyses were performed. The morphology of graphene oxide and bentonite/graphene oxide before and after sorption is shown in SEM pictures in (Fig.

1). the surface morphology of GO (Fig.1a) was changed, referring to localize bentonite particles (Fig. 2b). After adsorption (Fig.1c), modified GO surfaces became swollen. The adsorption of metal ions could be the cause of this swelling. After adsorption, the surface morphology of bentonite/GO was rougher than before the sorption process. Bentonite/GO had some fluffy feathers attached to it. This discovery revealed that the interaction of functional groups with metal ions could result in the formation of precipitates or complexes on the adsorbent's surface. The EDAX pattern of the bentonite/graphene oxide (Fig.2a,b,c) mixtures supported this result. Cu(II) and Zn(II) were adsorbed by bentonite/ GO, as evidenced by the increase in the metal peak in the EDAX pattern of bentonite/ GO following sorption (Fig.2c).

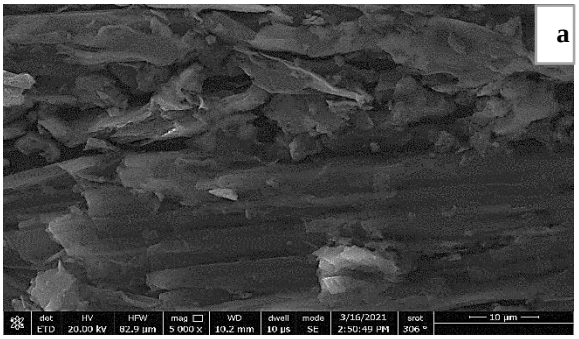

Fig 1a. SEM image of GO

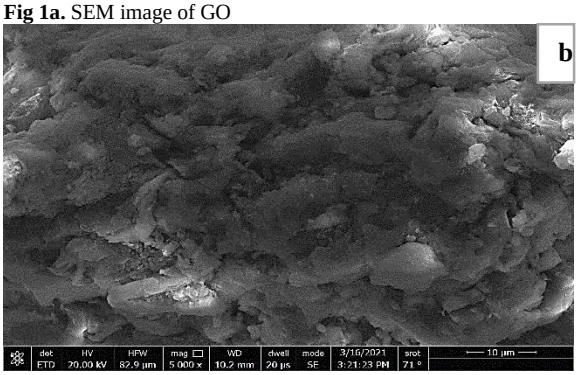

Fig 1b. SEM image of B/GO before sorption

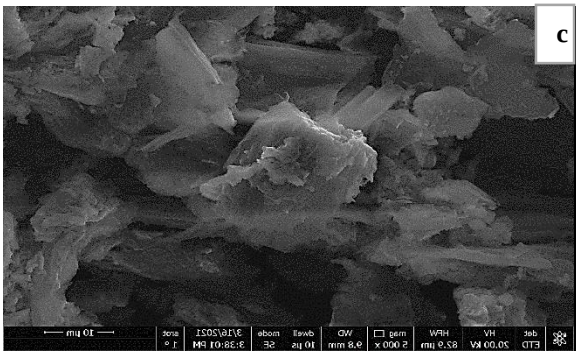

Fig 1c. SEM image of B/GO after sorption

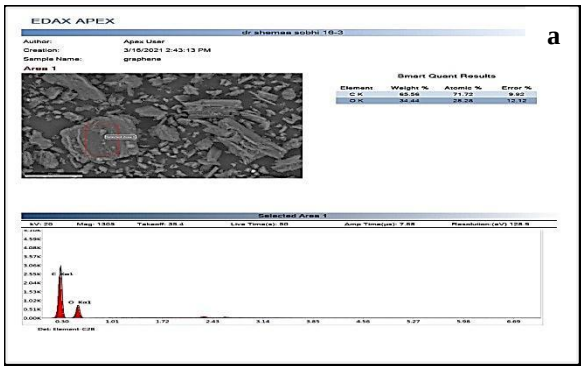

Fig 2a. EDAX image of GO

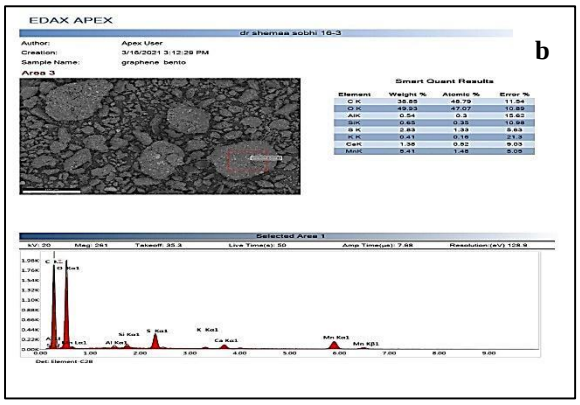

Fig 2b. EDAX image of B/GO before sorption

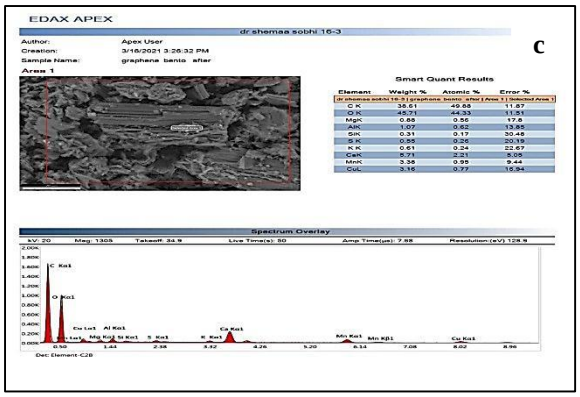

Fig 2c. EDAX image of B/GO after sorption

3.1.2. XRD analysis:

X-ray diffraction technique (XRD) usage yielded information about spacing mineral basal, proved adsorption facts, and revealed the adsorbed molecules into the GO particle basal spacing.

The XRD patterns of graphene oxide, bentonite/ GO, and bentonite/ GO after adsorption showed in Fig.3a,b,c. GO exhibited a diffraction peak at $2\theta=10.7$ that can be attributed to The formation of oxygen-containing groups on outside edges causing an increase in interlayer spaces and the production of apparent diffraction peaks, as illustrated in Fig.3a

[35,36]. Fig.3b. Indicates that the one of bentonite/ GO changed to 2θ =10.2 after the formation of bentonite/ GO.

Fig.3c.indicates that the peak of bentonite/ GO changed to 2θ = 4.825 after metal ion adsorption. According to Bragg's law ƛ = 2d sinθ, the layer spacing of bentonite/ GO increased to 1.55 nm from 1.52 nm of GO, indicating that bentonite has agglomerated into GO by cation exchange. As a result, the layer spacing of GO enlarged.

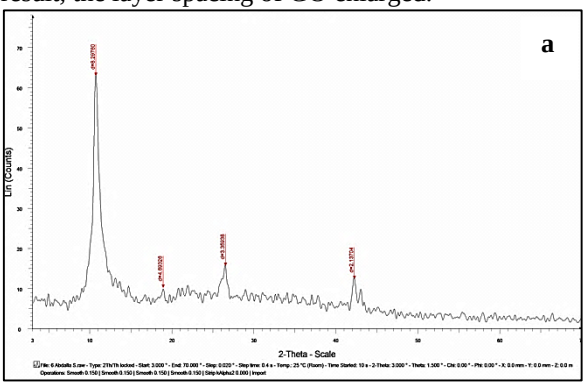

Fig 3a. the XRD pattern of GO

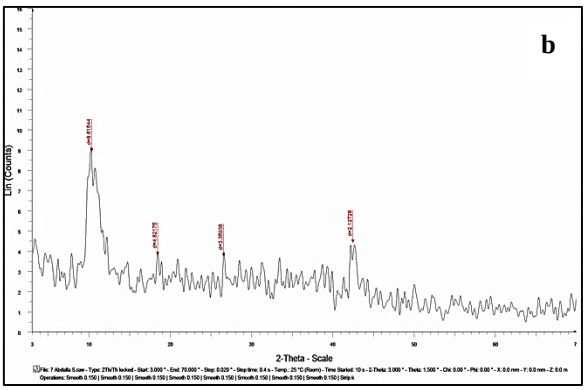

Fig 3b. the XRD pattern of bentonite/ GO before adsorption

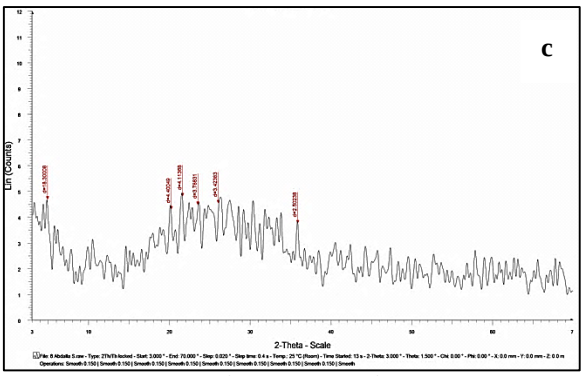

Fig 3c. the XRD pattern of bentonite/ GO after adsorption

3.1.3. FTIR analysis:

Figure.4 shows the FTIR spectra of GO, bentonite/GO before and after adsorption. GO observed its major distinctive peaks at 3346, 1716, 1618, 1384, and 1052 cm^{-1}. The stretching vibrations of –OH bonds caused the broad peak near 3346 cm^{-1}, the stretching vibrations of –COOH bonds caused the broad peak at 1716 cm^{-1}, and the stretching vibration of the C=C stretching vibration peak caused the broad one at 1618 cm^{-1}. These were at 1384 and 1052 cm^{-1}, respectively, coresponding to C–OH characteristic peaks and C–O stretching vibration ones [34]. The main characteristic peaks of graphene oxide were observed in the Spectral data of bentonite/GO in the region of 450–4000 cm^{-1}. The major component of bentonite/GO is indicated. The FTIR spectra of bentonite/GO revealed that the C–O peak (1052 cm^{-1}) on GO moved and overlapped to 1049 cm^{-1} compared to that of GO.

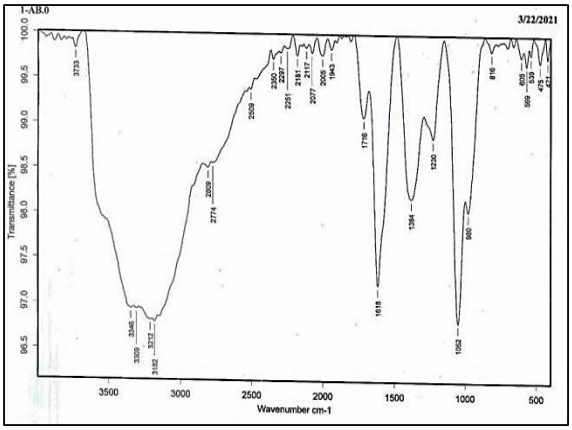

Fig 4a. FTIR spectra of GO

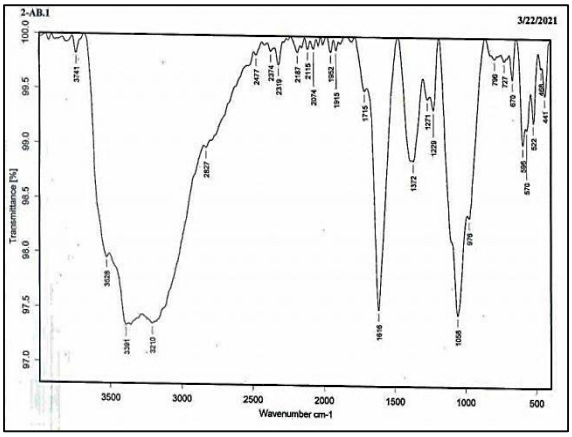

Fig 4b. FTIR spectra of bentonite/ GO before adsorption

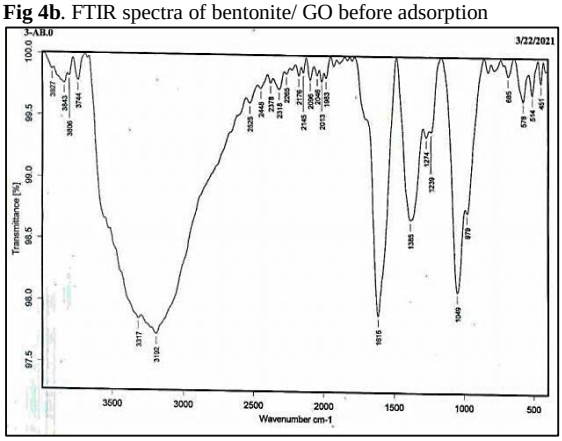

Fig 4c. FTIR spectra of bentonite/ GO after adsorption.

3.1.4. TEM analysis:

The morphology structure of bentonite/GO showed in Fig.5. Because of their irregular edges and single-layered construction, bentonite/GO films appear to be transparent. Bentonite particles localized on the graphene oxide surface. Bentonite/GO had a rough surface with many irregular wrinkles, which could be due to the different carboxyl and hydroxyl functional groups formed during the oxidation process [37].

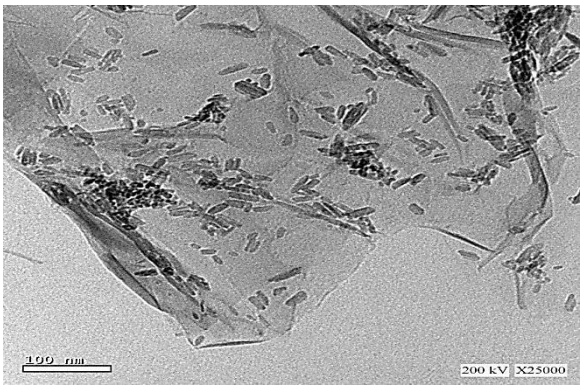

Fig 5. TEM image of modified bentonite/GO

3.2. Batch studies

3.2.1. pH Influence on the adsorption process:

The pH values have a remarkable impact on the absorbent's surface charge and the metal ion's ionization in an aqueous solution [38]. pH effects on Zinc and Copper sorption by bentonite/GO from 2 to 12 were investigated. The results are shown in Fig.6. The rate of Zn(II) and Cu(II) ion removal by bentonite/GO is almost influenced by pH. As the pH raised from 2 to 5.6, Copper sorption increased rapidly, plateaued, and subsequently dropped. At pH 5.6, the highest removal rate of Copper and Zinc by bentonite/GO is 99.75 % and 99.79 %, respectively, according to experimental results (as optimum pH value). In comparison to recorded data obtained from ref [39]: at pH 6, over 60-min adsorption time, the highest removal efficiency of Cu2+ on graphene oxide is 97.4%. Cu(II) ion removal rate gradually declined as pH increased from 7.0 to 9.0 until pH 9.0 was reached. The removal rate of Cu(II) and Zn(II) ions on bentonite/GO is too low at low pH values (2–3), according to pH data. That could be due to the conflict for active sites in bentonite/GO between H_3O^+ and metal ions. The available concentration of H_3O^+ reduced as the pH climbed from 2 to 5.6, competing with Zn(II) and Cu(II) ions for active sites on the bentonite/GO, increasing the removal rate. Because the Cu(II) and Zn(II) ions are dominant in the solutions without any concentrations of $H3O^+$ and the metal ions are still soluble, Cu(II) and Zn(II) removal rates on GO and bentonite/GO are stable or minimally varied in the pH range of 5.6 to 7. When the pH exceeds 7, however, copper as $Cu(OH)_2$ and zinc as $Zn(OH)_2$ precipitation is more likely to control than Cu(II) and Zn(II) ions, even though adsorption and coprecipitation are identical [40]. Reference [41] has more information on copper ion speciation in aqueous solutions as a function of pH. To avoid any precipitation of Cu(II) and Zn(II) ions, accomplishment experiments were carried out at pH 5.6 to assure metal ion solubility. As can be seen in Fig.7. Due to the presence of a complete charge balance between the equilibrated ions in an aqueous solution, there were no surface charges to be neutralized at the pHzpc value. The surface became charged positively when the pH was lower than the pHzpc threshold. It became negatively charged at a pH higher than pHzpc [42]. Terminal OH and NHCOO groups were used to determine the pHzpc value, which was based on functional groups that were most membrane structures.

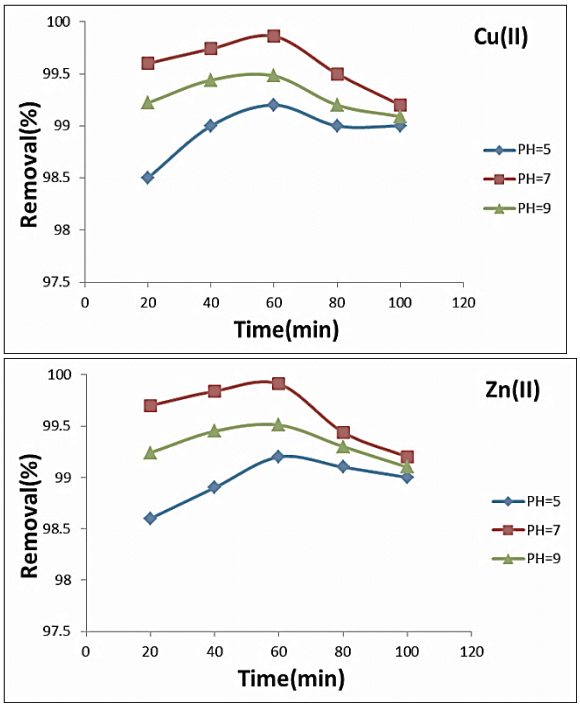

Fig.6. pH Influence on adsorption of Cu(II) and Zn(II) on B/ GO at different times(0.5g/L, 10ppm, 25 ± 2 °C, 200rpm).

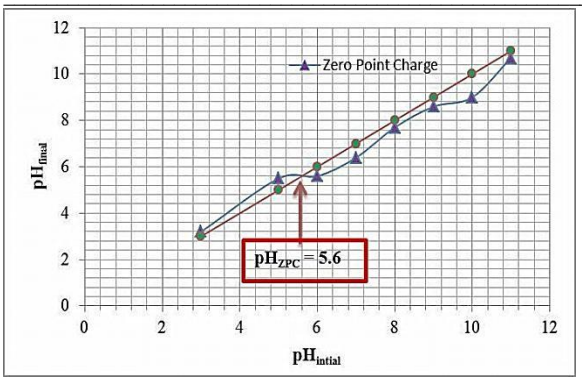

Fig.7. zero-point charge curve.

3.2.2. Contact time Effect:

The contact time influence was investigated in the range of (10 to 120 min) just using an initial concentration of 10, 15, 20, 25, and 30 mg/L of bentonite/GO, respectively, for a pH of 5.6 at room temperature to describe sorption rate and evaluate the equilibrium time for Cu(II) and Zn(II) sorption onto bentonite/GO. Figure.8. illustrates the time effect on Zinc and Copper sorption on bentonite/GO. Generally, the Copper and Zinc removal rate increased noticeably as the duration time increased from 0 to 45 minutes, reaching equilibrium after 45 minutes with no additional rises. According to the data collected, the amount of Zinc and Copper adsorbed on bentonite/GO became very fast within the first 15 minutes, and the bentonite/GO removal rate was (86.84 %). The initial sorption step in this situation causes Zinc and Copper ions to come into contact with a large number of accessible active surface sites of bentonite/GO. As the duration time raised (after 15 minutes), the number of accessible unoccupied active sites reduced, slowing the adsorption process, making it take longer to reach the equilibrium of adsorption, and weakening the removal rate. Bentonite/GO removal rate is significantly greater than for GO, which could be since there are more surface active sites of bentonite/GO than on the surface of GO. Furthermore, the negatively charged ions of bentonite/GO interact with metal ions more readily than hydroxyl groups and epoxy in the case of GO. Based on the mentioned findings, we've decided that 45 minutes is the best contact time for the coming trials. The refs [42142,44] produced similar results.

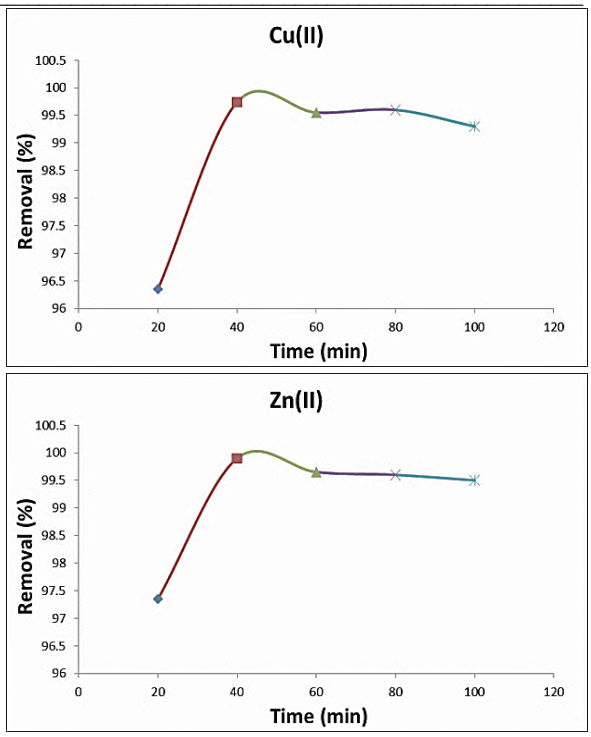

Fig.8. Effect of time on adsorption of Cu(II) and Zn(II) on B/ GO at (pH=5.6, 45 min, 0.5g/L, 20ppm, 25 ± 2 °C, 200rpm).

3.2.3. concentration Effects:

The adsorbate mass transfer barrier from the solution bulk to the sorbent surface is described by the concentration of initial metal ions [37]. The influence of Copper and Zinc initial concentrations ranging from 10 to 30 mg/L on the removal rate is shown in Figure 9. According to the results, the removal effectiveness of Copper and Zinc ions was reduced as the initial concentration for bentonite/GO was increased. Furthermore, at an initial Copper and Zinc concentration of 20 mg/L, the maximum removal rates for Cu(II) and Zn(II) were 99.75 percent and 99.79 percent, respectively. Then, when the initial concentration rises, the removal efficacy quickly drops. In contrast, when the Copper and Zinc initial concentration increased, the sorption capacities (Qe, mg/g) for them also increased, with maximum sorption capacities of 39.896 and 39.954 for Cu(II) and Zn(II), respectively. The initial concentration impact behaves similarly to that described in Ref. [45]. According to the findings, when the Copper and Zinc initial concentrations increased, the removal effectiveness declined. This could be owing to a lack of binding sites for additional metal ions to adsorb, resulting in a decrease in adsorption [45]. In addition, the initial Copper concentration has a direct influence

on Copper diffusion from the solution bulk to the bentonite/GO surface [46]. The concentration effect of Copper and Zinc ions on the removal rate of sorption at different times showed in Fig.9. The concentration of Cu(II) and Zn(II) ions is 10, 15, 20, 25, and 30 mg/L. 0.025g of bentonite/ GO is added to different concentrations of metal ions (50 ml). The removal time, pH, and temperature are 45 min, 5.6, and 25°C, respectively. The removal rate of Copper and Zinc ions decreases with increasing concentration. When the concentration of metal ions is 30 mg/L, the Cu(II) and Zn(II) ions removal rate by bentonite/ GO is 87.4% and 87.82%, respectively.

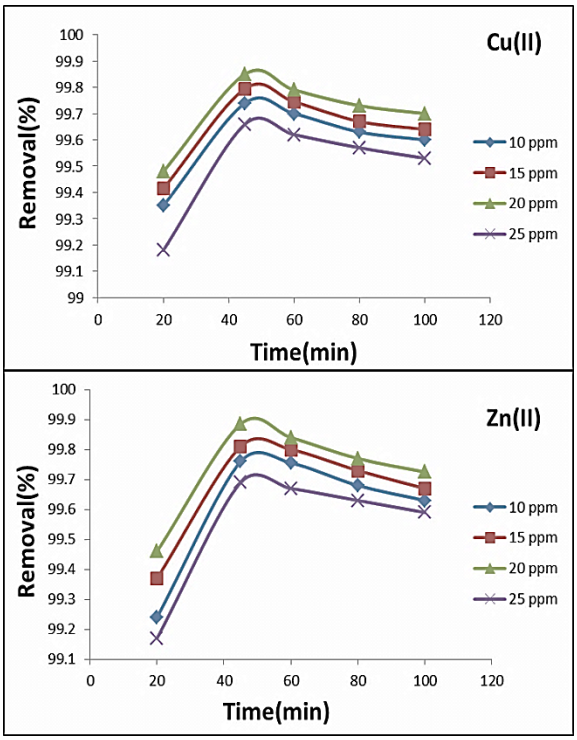

Fig.9. Removal efficiency of Cu(II) and Zn(II) on B/GO with different concentration at different times (pH=5.6, 0.5g/L, 25 ± 2 °C, 200rpm).

3.2.4. Effect of temperature:

As shown in Fig.10. The best temperature is 25 °C. When the temperature rises, the excessive temperature may cause the decomposition of bentonite/GO reducing the Zn(II) and Cu(II) ions removal rate. It is vital to consider that in most processes and chemical reactions, every change in the temperature range of the reaction affects the effectiveness of desorption or adsorption on a surface. As a result, the temperature is an essential physicochemical variable that affects adsorption processes [56]. To evaluate the temperature influence: it is essential to calculate the thermodynamic parameters, which include Gibbs free energy, enthalpy, and entropy. ΔG° and ΔH° are used to judge whether the adsorption is spontaneous and endothermic, as well as the value of ΔS° represents the randomness of the solution [57].

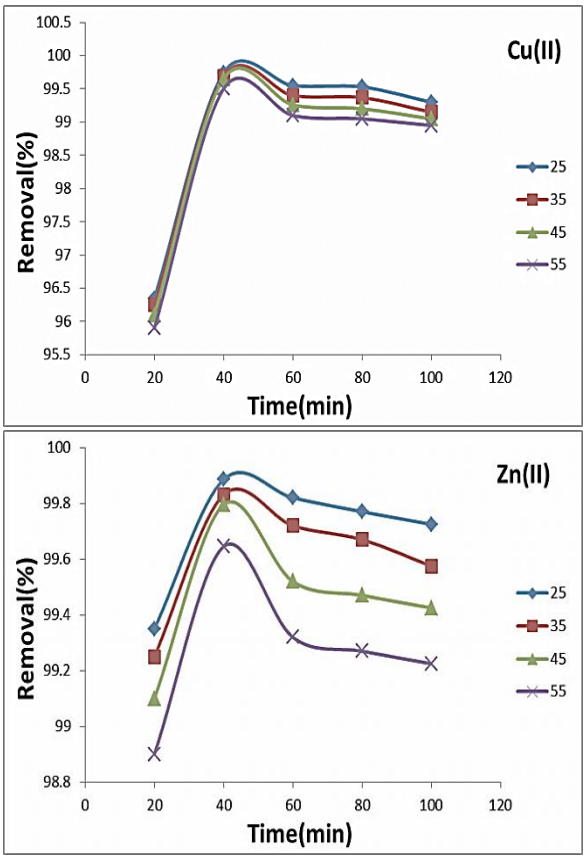

Fig.10. Effect of temperature on removal efficiency of Cu(II) and Zn(II) on B/GO at different times (pH=5.6, 0.5g/L, 20ppm, 200rpm).

3.2.5. Adsorbent dosage effect:

The influence of adsorbent mass was determined by changing the bentonite/ GO amount from 0.1 to 1 g/L on the adsorption of Cu(II) and Zn(II) ions solution (20 mg/L, stirring 200 rpm, pH 5.6 and Temp 25 °C). Figure.11. displayed an increase in the removal efficiency with the adsorbent mass increasing up to 0.5 g/L and then decreasing. Hence, the optimum bentonite/ GO mass for adsorption of Cu(II) and Zn(II) ions are 0.5 g/L. Due to the agglomeration and particle interactions that limit active sites, a limitation of surface area was observed while increasing the adsorbent dosage [45,46].

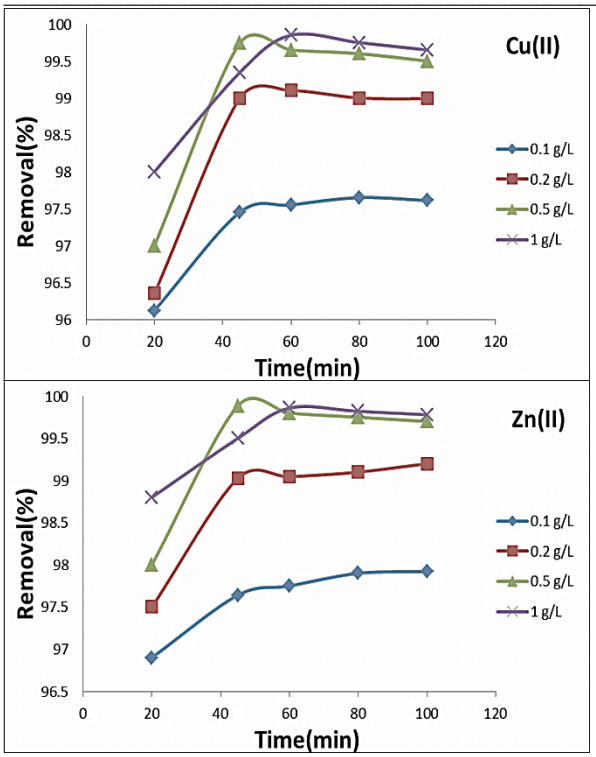

Fig.11. Adsorbent dosage influence on removal efficiency of Cu(II) and Zn(II) on B/GO at different times (pH=5.6, 20ppm, 25 ± 2 °C, 200rpm).

3.2.6. Kinetic studies:

Kinetic models are essential for verifying the probable metal ion adsorption mechanism as well as adjusting the rate of adsorption. Using various kinetic models, illustrate the Cu(II) and Zn(II) ions adsorption kinetics on (B/GO). Three kinetic Formulas, namely; pseudo-first-order, pseudo-second-order, and Ritchie's second-order Equations, were used to evaluate the experimental kinetic data, while four intraparticle diffusion Equations, namely; Morris–Weber, Bangham, Elovich, and Reichenberg Equations, were used to investigate the intraparticle diffusion. The models with the highest linear regression correlation (R^2) were deemed the best strategy for describing experimental kinetics of metal adsorption [45,49,50].

The following equations represent the linearized forms of Lagergren's pseudo-first-order, Ho's pseudo-second-order, and Ritchie's second-order kinetics, respectively [47,49,50]:

Pseudo-first order [51];

$$\log(q_e - q_t) = \log q_e - K_1\, t \quad (3)$$

Pseudo-second-order [49,46],

$$t/q_t = 1/K_2 q_e{}^2 + t/q_e \quad (4)$$

Ritchie's second order [52].

$$1/q_t = 1/K q_e t + 1/q_e \quad (5)$$

Where q_e and q_t are the equilibrium adsorption capacities (mg/g) at any adsorption time by minutes (t). K_1 (min^{-1}), K_2 (g $mg^{-1}min^{-1}$), and K are rate constants for the pseudo-first-order, pseudo-second-order, and Ritchie's second-order, respectively. Ho is the initial sorption rate for pseudo-second-order Equation (ho = K_2qe^2).

All adsorption aspects (surface adsorption, external film diffusion, and internal particle diffusion) are classified as pseudo-second-order kinetics. As a result, the rate-controlling phase of the sorption process had to be identified. The following are the intraparticle diffusion Equations that were studied as follows; Model Morris–Weber [53];

$$q_t = K_i t^{1/2} + C \quad (6)$$

Elovich Equation [54].

$$q_t = \frac{1}{\beta ln(\alpha\beta)} + \frac{1}{\beta lnt} \quad (7)$$

The metal ion adsorbed amount at a definite time (t) is given by q_t (mg/g). Morris–Weber's rate constant is K_i (mg/g $min^{1/2}$) is for intraparticle diffusion; C is the intercept value for determining the boundary layer thickness. The Elovich constants α_e and β_e are related to the rate of chemisorption and the extent of surface covering. As shown in Fig.12 and 13, the slopes and intercepts of the linear plots were used to estimate the kinetic parameters for Copper and Zinc adsorption via (B/GO). Table (1,2) summarised the kinetic constant values. The regression coefficient of the pseudo-first-order equation for Cu(II) and Zn(II) ions is 0.9232 and 0.9348, respectively, based on the data in the Table. For Cu(II) and Zn(II) ions, the pseudo-second-order model's regression coefficient is 0.9987 and 0.9994, respectively. The pseudo-first-order model's regression coefficients (R^2) are lower than those of the pseudo-second-order model. The experimental values (Q_e exp.=39.896 and 39.954) did not agree with the estimated capacities (Q_e cal.=2.235 and 0.5735) from the pseudo-first-order model for Cu(II) and Zn(II) ions. The pseudo-second-order model's calculated capabilities (Q_e cal.) are similar to the experimental results (Q_e cal.=40 and 39.84). As a result, the pseudo-second-order kinetic model could accurately describe the experimental results of Copper and Zinc adsorption on (B/GO).

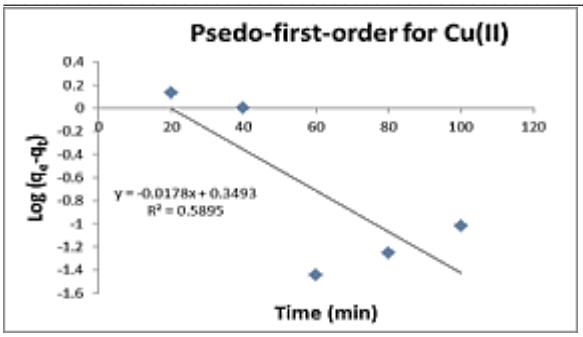

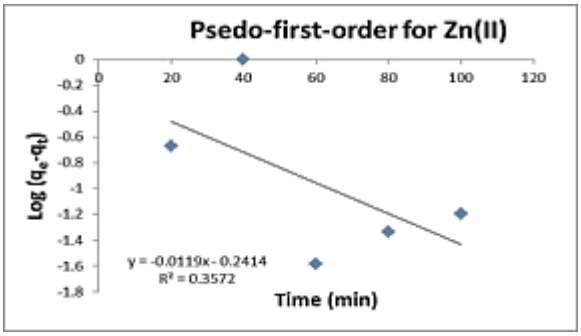

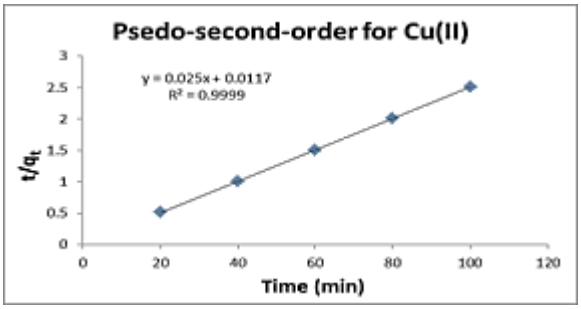

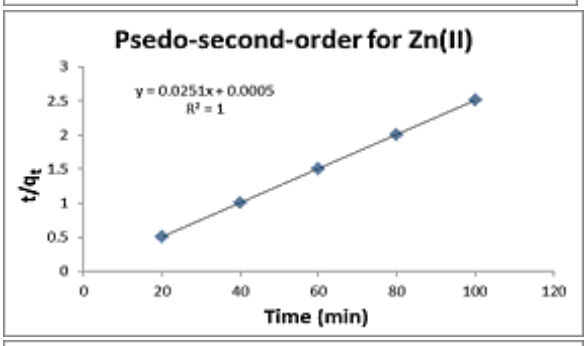

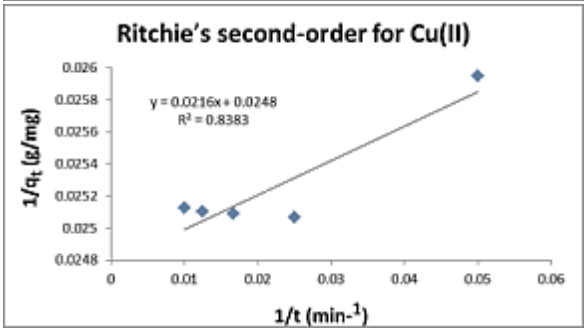

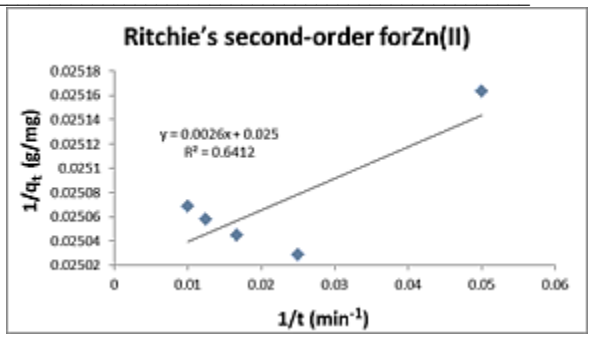

Fig.12. plot of pseudo-first-order, pseudo-second-order, Ritchie's second-order equations for Cu(II) and Zn(II) adsorption on B/GO surface. Co 20 mg/L of solution; temperature: 298 K, at pH 5.6.

Table 1
Parameters and regression coefficients (R2) of Kinetic models experimental data for Zn(II) and Cu(II) ions adsorption on B/GO surface. Co 20 mg/L of solution; temperature: 298 K, at pH 5.6.

Kinetic Equation	Constants	Cu(II)	Zn(II)
Pseudo-first-order	Slope	-0.0178	-0.0119
	Intercept	0.3493	-0.2414
	R^2	0.5895	0.3572
	$K_1(min^{-1})$	-0.04099	-0.0274
	$Q_{cal}(mg/g)$	2.235	0.5735
Pseudo-second-order	Slope	0.025	0.0251
	Intercept	0.0117	0.0005
	R^2	0.9999	1
	$K_2(min^{-1})$	0.0534	50.2
	$Q_{cal}(mg/g)$	40	39.8406
Ritchie's second-order	Slope	0.0216	0.0026
	Intercept	0.0248	0.025
	R^2	0.8383	0.6412
	$K(min^{-1})$	1.1481	9.6153
	$Q_{cal}(mg/g)$	40.3225	40

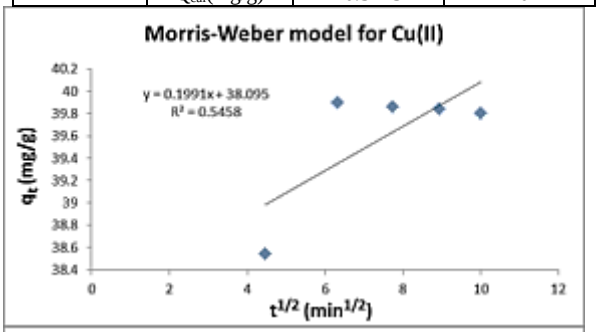

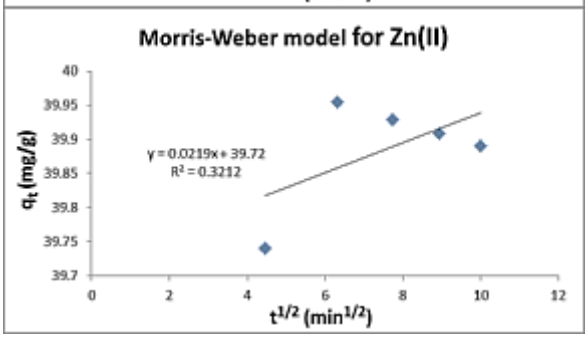

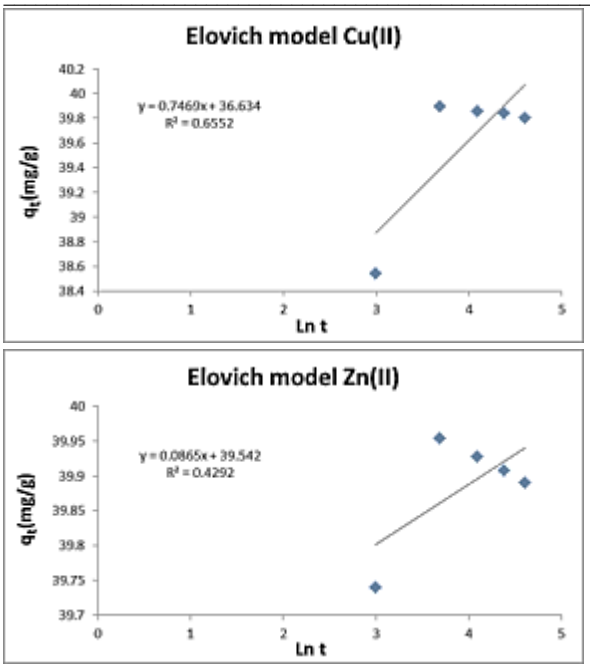

Fig.13. plot of intraparticle diffusion Morris–Weber and Elovich equations for Cu(II) and Zn(II) adsorption on B/GO surface. Co 20 mg/L of solution; temperature: 298 K, at pH 5.6.

Table 2

Parameters and regression coefficients (R2) of Kinetic models intraparticle diffusion Equations for Zn(II) and Cu(II) ions adsorption on B/GO surface. Co 20 mg/L of solution; temperature: 298 K, at pH 5.6.

Intraparticle Diffusion Equation	Constants	Cu(II)	Zn(II)
Morris–Weber	Slope	0.1991	0.0219
	Intercept	38.095	39.72
	R^2	0.5458	0.3212
	K_i(mg/g $min^{1/2}$)	0.1991	0.0219
	C	38.095	39.72
Elovich	Slope	0.7469	0.0865
	Intercept	36.634	39.542
	R^2	0.6552	0.4292
	β_e(g/mg)	1.3388	11.56069
	Lin($\alpha\beta$)	0.02038	0.002187
	$\alpha\beta$	$8.8528x10^{-3}$	1.00218
	α_e(mg/g min)	$6.6122x10^{-3}$	0.08668

3.2.7. Adsorption isotherm models

To verify the equilibrium investigations for metal ions removal from the solution, various mathematical models were applied [58]. The Langmuir, Freundlich, and Temkin isotherms are the most often used to characterize the equilibrium solid-liquid system. According to the Langmuir model, metal adsorption happens as monolayers on a homogeneous surface. Eq. (8) shows the linearized expression of the Langmuir adsorption isotherm. [58] :
given by [61]:

$$\frac{C_e}{Q_e} = \frac{1}{K_L Q_{max}} + \frac{C_e}{Q_{max}} \quad (8)$$

Where the adsorption capacity (mg/g) at equilibrium is Q_e, the liquid-phase (mg/L) of Copper concentration is C_e, Q_{max} is the maximum adsorption capacity adsorbent, and K_L is the Langmuir adsorption constant by (L/mg) related to the adsorption energy.

The intercept and slope of the graph plotted of C_e/Q_e VS C_e, respectively, can be used to determine these constants.

The non-dimensional sorption coefficient (R_L) defined as

$$R_l = \frac{1}{1 + K_L Co}$$

There are four types of sorption based on the R_L value: (1) favourable sorption when $0 < R_L < 1$, (2) unfavourable sorption when $R_L > 1$, (3) linear sorption when $R_L = 1$, and (4) irreversible sorption when $R_L = 0$ [55]. Cu(II) R^2 values range from 0.9884 to 1, while Zn(II) R^2 values vary from 0.9881 to 1, suggesting acceptable linearity.

In addition, the data were fitted to the Freundlich model, which is characterized by the linear equation given by Eq. (4):

$$\log Q_e = \log K_f + \frac{1}{n} \log C_e \quad (9)$$

The Freundlich parameters indicate the sorption capacity (density) and sorption intensity, whitch correspondingly, are the intercept (K_f) and the slope derivative (n). The higher values of K_f, the more heterogeneity, and the higher value of n (n > 1), the more spontaneously the sorption process is.

Results demonstrate that (n) values are less than 1, for Cu(II) vary from -20.08 to -4.26, while for Zn(II) range from -27.62 to -4.046, showing that metal ions sorption on(B/GO) is not suitable. Freundlich constants indicate that difficult metal ions removal from aqueous solution.

The Temkin model assumes that the sorption heat is linear rather than logarithmic, as shown in Freundlich's equation. It's written as [59]:

$$q_e = \frac{RT}{b} \ln(K_T C_e) = B_1 \frac{RT}{b} \ln(K_T C_e) \quad (10)$$

According to the Temkin model, the decrease in sorption temperature was linear rather than logarithmic, as predicted by the Freundlich model [60].

Equation (5) is used to produce the linear plot of Q_e VS ln C_e for the Temkin model.

$$q_e = \frac{RT}{b_T}\ln(C_e) + \frac{RT}{b_T}\ln(K_T) \qquad (11)$$

Where constant $B_1 = RT/b$ is related to the adsorption heat constant. R is the general gas constant (J mol^{-1} K^{-1}), T is the temperature (K), b is the adsorption energy variation (J mol^{-1}), and K_T is the equilibrium binding constant (Lmg^{-1}) consistent with the highest binding energies.

3.2.8. Sorption thermodynamics

Equilibrium constants varying with temperature are used to estimate thermodynamic parameters such as enthalpy change (ΔH°), Gibbs free energy change (ΔG°), and entropy change (ΔS°). Table (5) shows the assessment results of standard Gibbs free energy change for the biosorption process using b obtained results from the Langmuir model at various temperatures [62]. The sorption reaction Gibbs free energy change is described by the equation below.

$$\Delta G^{o} = -RT\ln b = -RT\ln K$$

The universal gas constant (8.314 $Jmol^{-1}$ K^{-1}) is represented by R. T, on the other hand, is the absolute temperature in Kelvin. The negative value of ΔG° verifies the efficiency of the procedure and the metal ion adsorption spontaneous nature with a high metal ions affinity for bio-sorbent, as shown in Tables (5). The equilibrium constants can be represented as follows in terms of enthalpy change of temperature adsorption:

$$\frac{d\ln K}{dT} = \frac{\Delta H^{o}}{RT^{2}}$$

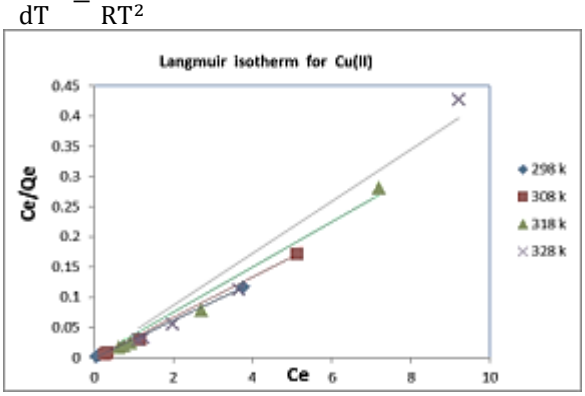

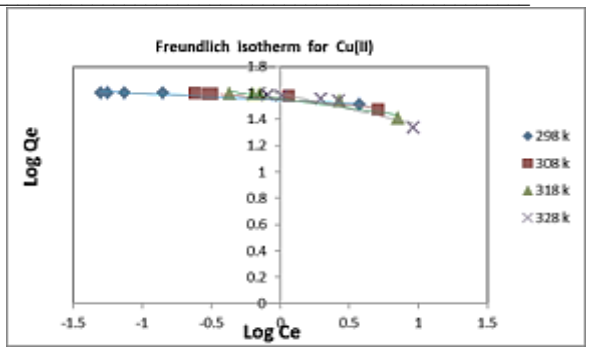

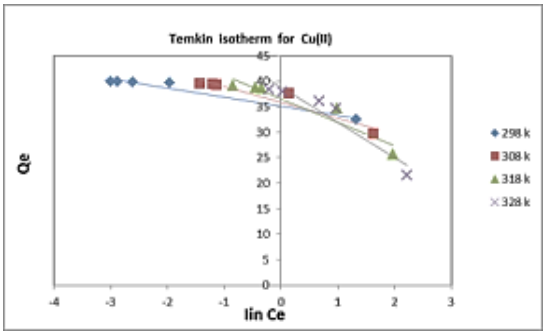

Fig 14. Langmuir, Freundlich and Temkin models for Cu(II) ions sorption on B/GO.

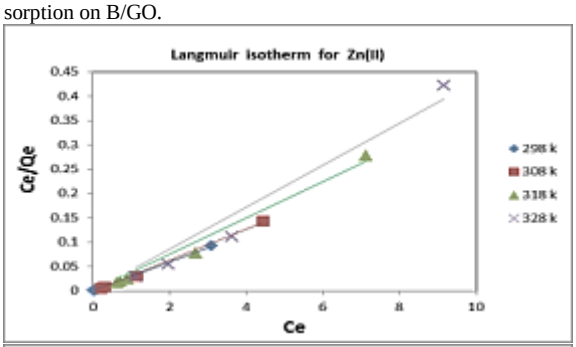

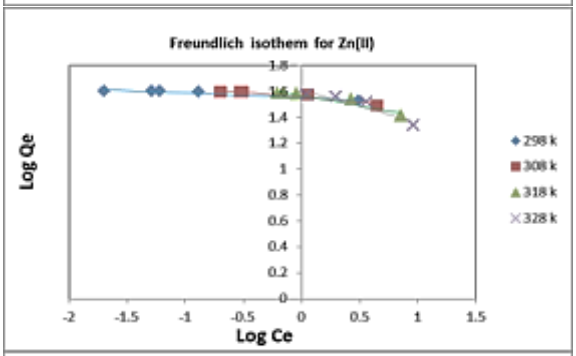

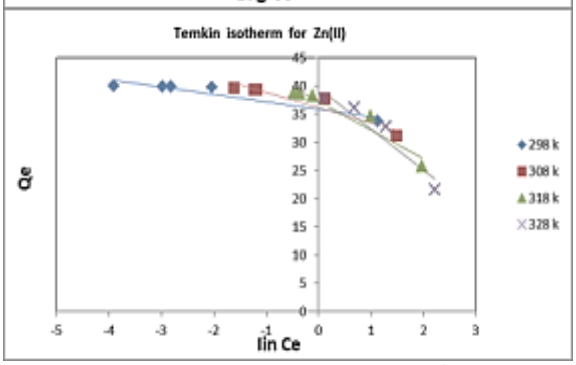

Fig 15. Langmuir, Freundlich and Temkin models for Zn(II) ions sorption on B/GO.

Table 3 : Shows the results of Langmuir, Freundlich and Temkin models for Cu(II) ions.

Cu (II) adsorption Isotherm Parameters and correlation coefficient of Langmuir, Freundlich and Temkin models at different temperatures.									
Temperature (K)	**Langmuir**			**Freundlich**			**Temkin**		
	Q_{max}	K_L	R^2	K_f	n	R^2	K_T	b_T	R^2
298	32.362	61.8	1	34.922	-20.0803	0.9587	341114358.1	-1381.109	0.9595
308	29.239	8.7692	0.9985	35.636	-11.1607	0.8907	$9.075X10^{-6}$	-828.066	0.9027
318	24.752	2.7482	0.9933	36.266	-6.9735	0.8808	$3.749X10^{-4}$	-570.545	36.568
328	20.202	1.2659	0.9884	39.336	-4.2625	0.8773	$3.642X10^{-3}$	-394.273	38.842

Table 4: Shows the results of Langmuir, Freundlich and Temkin models for Zn(II) ions

Zn (II) adsorption Isotherm Parameters and correlation coefficient of Langmuir, Freundlich and Temkin models at different temperatures.									
Temperature (K)	**Langmuir**			**Freundlich**			**Temkin**		
	Q_{max}	K_L	R^2	K_f	n	R^2	K_T	b_T	R^2
298	33.670	-99	1	35.7272	-27.624309	0.8981	$2.7935X10^{-12}$	-1863.1163	0.8995
308	30.674	-10.8666	0.9986	35.9749	-13.227513	0.8829	$1.3181X10^{-6}$	-958.7091	0.8949
318	24.937	-2.8239	0.9934	37.0766	-6.3171194	0.9014	$6.6860X10^{-4}$	-519.14544	0.9246
328	20.366	-1.3128	0.9881	40.41103	-4.0469446	0.8915	$4.2916X10^{-3}$	-375.7999	0.924

As seen in Eq (8), the sign of H° determines the temperature effect on the equilibrium constant b. As a result, when (ΔH°) is positive, i.e. when adsorption is endothermic, a rise in T occurs increases (K). An increase in T induces a drop in K when (ΔH°) is negative, i.e. when the adsorption is exothermic chemisorption [63]. The equilibrium constant and the free energy change are expressed as follows as a function of temperature.

$$\ln K_d = (\Delta H/RT) + (\Delta S/R) \quad (12)$$

$$\Delta G = \Delta H - T\Delta S \quad (13)$$

$$\Delta H = E_a - RT \quad (14)$$

Where K_d is the metal sorption distribution coefficient. H° denotes the change in enthalpy, G indicates the change in Gibbs energy, S represents the change in entropy, E_a means the activation energy, R signifies the universal gas constant, and T refers to the absolute temperature. Estimating intercept and slope values of the linear plot of ln k_d against 1/T yields all of the thermodynamic parameters as evaluated in Table (5). Under equilibrium conditions in the batch process, Figure (14) showed a linear correlation between ln K_d and 1/T for Cu(II) (R^2 = 0.9692) and Zn(II) (R^2 = 0.9698) sorption onto (B/GO). As seen in Table (5), the ΔH° changes of Cu(II) bio-sorption on (B/GO) were -104.76 $kJmol^{-1}$ while ΔS° was -319.4 $Jmol^{-1}$ K^{-1}. The exothermic adsorption character was suggested by negative ΔH° values [64]. As shown in Table (5), the ΔH° changes of Zn(II) bio-sorption on (B/GO) were -117.01 $kJmol^{-1}$ while ΔS° was -357.11 $Jmol^{-1}$ K^{-1}. The exothermic adsorption character was suggested by negative ΔH° values [62]. This is confirmed by the fact that as the temperature rises, the bio-sorption sorbent's capacity value increases. Negative ΔS° (less disorder) results indicate that no changes in internal structures occur during the sorption process. The reducing randomness at the solid/liquid interface throughout metal sorption on the selected sorbent is shown in the negative values of ΔS°, which indicate the affinity of Zn(II) and Cu(II).

Due to the tiny values of Ea, H, the driving force such as functional groups chelation and proton displacement, the sorption process of metal ion onto (B/GO) was quick [65,66,67].

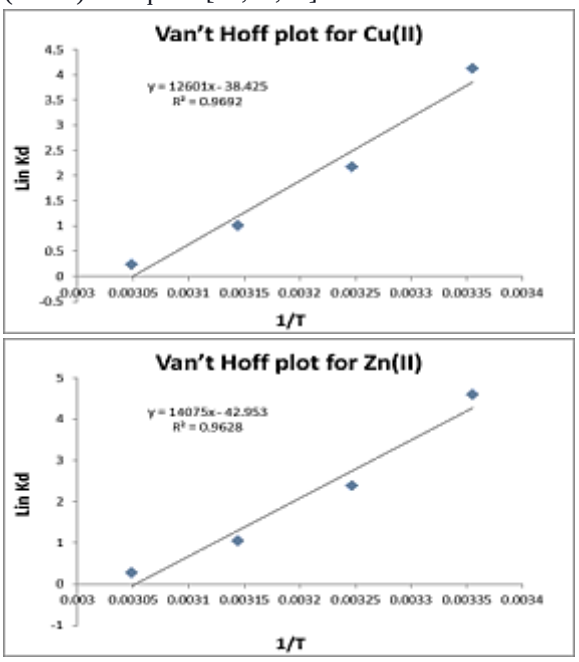

Fig 16. Showed a linear correlation between ln Kd and 1/T for Cu(II) and Zn(II) sorption onto (B/GO).

Table 5

Evaluation of thermodynamic parameters for Copper and Zinc ions.

Adsorbate	Temp (K)	Kd (L/mg)	ΔG°(kJ/mol)	ΔH° (kJ/mol)	ΔS°(J/K/mol)
Cu(II)	298	61.8	-10.21	-104.76	-319.46
	308	8.769	-10.56		
	318	2.748	-10.90		
	328	1.265	-11.24		
Zn(II)	298	99	-11.38	-117.01	-319.46
	308	10.86	-11.76		
	318	2.823	-12.14		
	328	1.312	-12.53		

4. Conclusions

This research aimed to examine the effectiveness and affordability of using modified GO nanoparticles to remove some heavy metals from aqueous solutions. It also evaluated the effects of various parameters, including dosage, temperature, contact time, pH, and initial metal concentration of the aqueous solution, on how well the adsorbent captured metal ions from the solution. To describe the adsorption equilibrium data, three isotherms models were used. In batch sorption mode, the selective separation behavior of the current adsorbent was studied.

5. Conflicts of interest

The authors declare that they have no conflicts of interst.

6. Acknowledgments,

Both authors would like to thank Menoufia University for its support in the present research and the required devices. Special thanks are devoted to the Central Laboratory staff for Environmental Quality Monitoring for their cooperation during measurements and for providing the necessary facilities to accomplish the work.

7. References

[1] Kołodyńska, D., Wnętrzak, R., Leahy, J. J., Hayes, M. H. B., Kwapiński, W., & Hubicki, Z. J. C. E. J. (2012). Kinetic and adsorptive characterization of biochar in metal ions removal. *Chemical Engineering Journal*, 197, 295-305.

[2] Chang, N. B., Houmann, C., Lin, K. S., & Wanielista, M. (2016). Fate and transport with material response characterization of green sorption media for copper removal via adsorption process. *Chemosphere*, 144, 1280-1289.

[3] Fu, F., & Wang, Q. (2011). Removal of heavy metal ions from wastewaters: a review. *Journal of environmental management*, 92(3), 407-418.

[4] Akbal, F., & Camcı, S. (2011). Copper, chromium, and nickel removal from metal plating wastewater by electrocoagulation. *Desalination*, 269(1-3), 214-222.

[5] Bilal, M., Shah, J. A., Ashfaq, T., Gardazi, S. M. H., Tahir, A. A., Pervez, A., ... & Mahmood, Q. (2013). Waste biomass adsorbents for copper removal from industrial wastewater—a review. *Journal of hazardous materials*, 263, 322-333.

[6] Liu, Q., Liu, Q., Ruan, Z., Chang, X., & Yao, J. (2016). Removal of Cu (II) from aqueous solution using synthetic poly (catechol-diethylenetriamine-p-phenylenediamine) particles. *Ecotoxicology and environmental safety*, 129, 273-281.

[7] Mullett, M., Fornarelli, R., & Ralph, D. (2014). Nanofiltration of mine water: impact of feed pH and membrane charge on resource recovery and water discharge. *Membranes*, 4(2), 163-180.

[8] Gonzalez, M. A., Trócoli, R., Pavlovic, I., Barriga, C., & La Mantia, F. (2016). Capturing Cd (II) and Pb (II) from contaminated water sources by electro-deposition on hydrotalcite-like compounds. *Physical Chemistry Chemical Physics*, 18(3), 1838-1845.

[9] Kong, D., Qiao, N., Liu, H., Du, J., Wang, N., Zhou, Z., & Ren, Z. (2017). Fast and efficient removal of copper using sandwich-like graphene oxide composite imprinted materials. *Chemical Engineering Journal*, 326, 141-150.

[10] Arán, D., Antelo, J., Fiol, S., & Macías, F. (2016). Influence of feedstock on the copper removal capacity of waste-derived biochars. *Bioresource technology*, 212, 199-206.

[11] Dreyer, D. R., Park, S., Bielawski, C. W., & Ruoff, R. S. (2010). The chemistry of graphene oxide. *Chemical society reviews*, 39(1), 228-240.

[12] Zhao, G., Wen, T., Chen, C., & Wang, X. (2012). Synthesis of graphene-based nanomaterials and their application in energy-related and environmental-related areas. *RSC Advances*, 2(25), 9286-9303.

[13] Luo, S., Xu, X., Zhou, G., Liu, C., Tang, Y., & Liu, Y. (2014). Amino siloxane oligomer-linked graphene oxide as an efficient adsorbent for removal of Pb (II) from wastewater. *Journal of hazardous materials*, 274, 145-155.

[14] Yang, S. T., Chang, Y., Wang, H., Liu, G., Chen, S., Wang, Y., ... & Cao, A. (2010). Folding/aggregation of graphene oxide and its application in Cu^{2+} removal. *Journal of colloid and interface science*, 351(1), 122-127.

[15] Xing, H. T., Chen, J. H., Sun, X., Huang, Y. H., Su, Z. B., Hu, S. R., ... & Huang, Y. (2015). NH_2-rich polymer/graphene oxide use as a novel adsorbent for removal of Cu (II) from aqueous solution. *Chemical Engineering Journal*, 263, 280-289.

[16] Vilela, D., Parmar, J., Zeng, Y., Zhao, Y., & Sánchez, S. (2016). Graphene-based microbots for toxic heavy metal removal and recovery from water. *Nano Letters*, 16(4), 2860-2866.

[17] Wang, H., Yuan, X., Wu, Y., Huang, H., Zeng, G., Liu, Y., ... & Qi, Y. (2013). Adsorption characteristics and behaviors of graphene oxide for Zn (II) removal from aqueous solution. *Applied Surface Science*, 279, 432-440.

[18] Li, Y., Du, Q., Liu, T., Sun, J., Wang, Y., Wu, S., ... & Xia, L. (2013). Methylene blue adsorption on graphene

oxide/calcium alginate composites. *Carbohydrate polymers*, 95(1), 501-507.

[19] Soroush, A., Ma, W., Cyr, M., Rahaman, M. S., Asadishad, B., & Tufenkji, N. (2016). In situ silver decoration on graphene oxide-treated thin film composite forward osmosis membranes: biocidal properties and regeneration potential. *Environmental Science & Technology Letters*, 3(1), 13-18.

[20] Wu, T., Cai, X., Tan, S., Li, H., Liu, J., & Yang, W. (2011). Adsorption characteristics of acrylonitrile, p-toluenesulfonic acid, 1-naphthalene sulfonic acid, and methyl blue on graphene in aqueous solutions. *Chemical Engineering Journal*, 173(1), 144-149.

[21] Ramesha, G. K., Kumara, A. V., Muralidhara, H. B., & Sampath, S. (2011). Graphene and graphene oxide as effective adsorbents toward anionic and cationic dyes. *Journal of colloid and interface science*, 361(1), 270-277.

[22] Li, Z., Chen, F., Yuan, L., Liu, Y., Zhao, Y., Chai, Z., & Shi, W. (2012). Uranium (VI) adsorption on graphene oxide nanosheets from aqueous solutions. *Chemical engineering journal*, 210, 539-546.

[23] Ren, X., Li, J., Tan, X., & Wang, X. (2013). Comparative study of graphene oxide activated carbon and carbon nanotubes as adsorbents for copper decontamination. *Dalton Transactions*, 42(15), 5266-5274.

[24] Yang, S., Okada, N., & Nagatsu, M. (2016). The highly effective removal of Cs^+ by low turbidity chitosan-grafted magnetic bentonite. *Journal of Hazardous Materials*, 301, 8-16.

[25] Wang, W., Zheng, B., Deng, Z., Feng, Z., & Fu, L. (2013). Kinetics and equilibriums for adsorption of poly (vinyl alcohol) from aqueous solution onto natural bentonite. *Chemical Engineering Journal*, 214, 343-354.

[26] Zong, P., Wu, X., Gou, J., Lei, X., Liu, D., & Deng, H. (2015). Immobilization and recovery of uranium (VI) using Na-bentonite from the aqueous medium: equilibrium, kinetics, and thermodynamics studies. *Journal of Molecular Liquids*, 209, 358-366.

[27] Ma, J., Qi, J., Yao, C., Cui, B., Zhang, T., & Li, D. (2012). A novel bentonite-based adsorbent for anionic pollutant removal from water. *Chemical Engineering Journal*, 200, 97-103.

[28] Van Tran, T., Bui, Q. T. P., Nguyen, T. D., Le, N. T. H., & Bach, L. G. (2017). A comparative study on the removal efficiency of metal ions (Cu^{2+}, Ni^{2+}, and Pb^{2+}) using sugarcane bagasse-derived $ZnCl_2$-activated carbon by the response surface methodology. *Adsorption Science & Technology*, 35(1-2), 72-85.

[29] Youssef, H. F., Nasr, R. A., Abou El-Anwar, E. A., Mekky, H. S., & Abd El Rahim, S. H. (2021). Preparation and characterization of different zeolites from andesite rock: Product evaluation for efficient dye removal. *Microporous and Mesoporous Materials*, 328, 111485.

[30] Smith, M., Ha, S., Amonette, J. E., Dallmeyer, I., & Garcia-Perez, M. (2015). Enhancing cation exchange capacity of chars through ozonation. *Biomass and Bioenergy*, 81, 304-314.

[31] Moradi, M., Dehpahlavan, A., Rezaei Kalantary, R., Ameri, A., Farzadkia, M., & Izanloo, H. (2015). Application of modified bentonite using sulfuric acid for the removal of hexavalent chromium from aqueous solutions. *Environmental Health Engineering and Management Journal*, 2(3), 99-106.

[32] Zaaba, N. I., Foo, K. L., Hashim, U., Tan, S. J., Liu, W. W., & Voon, C. H. (2017). Synthesis of graphene oxide using modified hummers method: solvent influence. *Procedia engineering*, 184, 469-477..

[33] Wang, H., Yuan, X., Wu, Y., Huang, H., Zeng, G., Liu, Y., ... & Qi, Y. (2013). Adsorption characteristics and behaviors of graphene oxide for Zn (II) removal from aqueous solution. *Applied Surface Science*, 279, 432-440.

[34] Ozdes, D., Duran, C., & Senturk, H. B. (2011). Adsorptive removal of Cd (II) and Pb (II) ions from aqueous solutions by using Turkish illitic clay. *Journal of Environmental Management*, 92(12), 3082-3090.

[35] Ansari, M. O., Kumar, R., Ansari, S. A., Ansari, S. P., Barakat, M. A., Alshahrie, A., & Cho, M. H. (2017). Anion selective pTSA doped polyaniline@ graphene oxide-multiwalled carbon nanotube composite for Cr (VI) and Congo red adsorption. *Journal of colloid and interface science*, 496, 407-415.

[36] Pham, V. H., Cuong, T. V., Hur, S. H., Oh, E., Kim, E. J., Shin, E. W., & Chung, J. S. (2011). Chemical functionalization of graphene sheets by solvothermal reduction of a graphene oxide suspension in N-methyl-2-pyrrolidone. *Journal of Materials Chemistry*, 21(10), 3371-3377.

[37] Park, K. W. (2014). Carboxylated graphene oxide–Mn_2O_3 nanorod composites for their electrochemical characteristics. *Journal of Materials Chemistry A*, 2(12), 4292-4298.

[38] Zhang, L., Lu, Z., Zhao, Q., Huang, J., Shen, H., & Zhang, Z. (2011). Enhanced chemotherapy efficacy by sequential delivery of siRNA and anticancer drugs using PEI-grafted graphene oxide. *Small*, 7(4), 460-464.

[39] White, R. L., White, C. M., Turgut, H., Massoud, A., & Tian, Z. R. (2018). Comparative studies on copper adsorption by graphene oxide and functionalized graphene oxide nanoparticles. *Journal of the Taiwan Institute of Chemical Engineers*, 85, 18-28.

[40] Li, Y., Yue, Q., & Gao, B. (2010). Adsorption kinetics and desorption of Cu (II) and Zn (II) from aqueous solution onto humic acid. *Journal of Hazardous Materials*, 178(1-3), 455-461.

[41] Xie, R., Jin, Y., Chen, Y., & Jiang, W. (2017). The importance of surface functional groups in the adsorption of copper onto walnut shell-derived activated carbon. *Water Science and Technology*, 76(11), 3022-3034.

[42] Moawed, E. A., & El-Shahat, M. F. (2014). Extraction of triazine herbicides by polyhydroxy-polyurethane foam in environmental samples. *Journal of chromatographic science*, 52(1), 12-18.

[43] Li, Y., Du, Q., Liu, T., Sun, J., Jiao, Y., Xia, Y., ... & Wu, D. (2012). Equilibrium, kinetic and thermodynamic studies on the adsorption of phenol onto graphene. *Materials Research Bulletin*, 47(8), 1898-1904.

[44] Jiang, T., Liu, W., Mao, Y., Zhang, L., Cheng, J., Gong, M., ... & Zhao, Q. (2015). Adsorption behavior of copper ions from aqueous solution onto graphene oxide–CdS composite. *Chemical engineering journal*, 259, 603-610.

[45] Wu, Q., Chen, J., Clark, M., & Yu, Y. (2014). Adsorption of copper to different biogenic oyster shell structures. *Applied surface science*, 311, 264-272.

[46] Massoud, A., Waly, S. A., & Abou El-Nour, F. (2017). Removal of U (VI) from simulated liquid waste using synthetic organic resin. *Radiochemistry*, 59(3), 272-279.

[47] Chen, D., Cheng, Y., Zhou, N., Chen, P., Wang, Y., Li, K., ... & Ruan, R. (2020). Photocatalytic degradation of organic pollutants using TiO_2-based photocatalysts: A review. *Journal of Cleaner Production*, 268, 121725.

[48] Jafari, S., & Nezamzadeh-Ejhieh, A. (2017). Supporting of coupled silver halides onto clinoptilolite nanoparticles as a simple method for increasing their photocatalytic activity in heterogeneous photodegradation of mixture of 4-methoxy aniline and 4-chloro-3-nitro aniline. *Journal of colloid and interface science*, 490, 478-487.

[49] Wu, Y., Luo, H., Wang, H., Wang, C., Zhang, J., & Zhang, Z. (2013). Adsorption of hexavalent chromium from aqueous solutions by graphene modified with cetyltrimethylammonium bromide. *Journal of colloid and interface science*, 394, 183-191.

[50] Wang, L., Yang, L., Li, Y., Zhang, Y., Ma, X., & Ye, Z. (2010). Study on adsorption mechanism of Pb (II) and Cu (II) in aqueous solution using PS-EDTA resin. *Chemical Engineering Journal*, 163(3), 364-372.

[51] Zhu, H. Y., Jiang, R., Xiao, L., & Zeng, G. M. (2010). Preparation, characterization, adsorption kinetics, and thermodynamics of novel magnetic chitosan enwrapping nanosized γ-Fe_2O_3 and multi-walled carbon nanotubes with enhanced adsorption properties for methyl orange. *Bioresource Technology*, 101(14), 5063-5069.

[52] Rahdar, S., Rahdar, A., Zafar, M. N., Shafqat, S. S., & Ahmadi, S. (2019). Synthesis and characterization of MgO-supported Fe–Co–Mn nanoparticles with exceptionally high adsorption capacity for Rhodamine B dye. *Journal of Materials Research and Technology*, 8(5), 3800-3810.

[53] Vinhal, J. O., Nege, K. K., Lage, M. R., Carneiro, J. W. D. M., Lima, C. F., & Cassella, R. J. (2017). Adsorption of the herbicides diquat and difenzoquat on polyurethane foam: Kinetic, equilibrium and computational studies. *Ecotoxicology and environmental safety*, 145, 597-604.

[54] Ahmad, M. A., Ahmad, N., & Bello, O. S. (2015). Removal of remazol brilliant blue reactive dye from aqueous solutions using watermelon rinds as adsorbent. *Journal of Dispersion Science and Technology*, 36(6), 845-858.

[55] Putra, W. P., Kamari, A., Yusoff, S. N. M., Ishak, C. F., Mohamed, A., Hashim, N., & Isa, I. M. (2014). Biosorption of Cu (II), Pb (II) and Zn (II) ions from aqueous solutions using selected waste materials: Adsorption and characterisation studies. *Journal of Encapsulation and Adsorption Sciences*, 2014.

[56] Mahmoud, M. E., Amira, M. F., Seleim, S. M., & Mohamed, A. K. (2017). Adsorption isotherm models, kinetics study, and thermodynamic parameters of Ni (II) and Zn (II) removal from water using the LbL technique. *Journal of Chemical & Engineering Data*, 62(2), 839-850.

[57] Vasudevan, S., & Lakshmi, J. J. W. S. (2011). Studies relating to an electrochemically assisted coagulation for the removal of chromium from water using zinc anode. Water Science and Technology: *Water supply*, 11(2), 142-150

[58] Sen, T. K., & Gomez, D. (2011). Adsorption of zinc (Zn^{2+}) from aqueous solution on natural bentonite. *Desalination*, 267(2-3), 286-294.

[59] Munagapati, V. S., & Kim, D. S. (2017). Equilibrium isotherms, kinetics, and thermodynamics studies for congo red adsorption using calcium alginate beads impregnated with nano goethite. *Ecotoxicology and environmental safety*, 141, 226-234.

[60] Singha, B., & Das, S. K. (2011). Biosorption of Cr (VI) ions from aqueous solutions: kinetics, equilibrium, thermodynamics and desorption studies. *Colloids and surfaces B: Biointerfaces*, 84(1), 221-232.

[61] Eloussaief, M., Kallel, N., Yaacoubi, A., & Benzina, M. (2011). Mineralogical identification, spectroscopic characterization, and potential environmental use of natural clay materials on chromate removal from aqueous solutions. *Chemical Engineering Journal*, 168(3), 1024-1031.

[62] Çelebi, H., Gök, G., & Gök, O. (2020). Adsorption capability of brewed tea waste in waters containing toxic lead (II), cadmium (II), nickel (II), and zinc (II) heavy metal ions. *Scientific reports*, 10(1), 1-12.

[63] Húmpola, P. D., Odetti, H. S., Fertitta, A. E., & Vicente, J. L. (2013). Thermodynamic analysis of adsorption models of phenol in the liquid phase on different activated carbons. *Journal of the Chilean Chemical Society*, 58(1), 1541-1544.

[64] Yadav, S., Srivastava, V., Banerjee, S., Weng, C. H., & Sharma, Y. C. (2013). Adsorption characteristics of modified sand for the removal of hexavalent chromium ions from aqueous solutions: Kinetic, thermodynamic and equilibrium studies. *Catena*, 100, 120-127.

[65] Dores, E. F., Spadotto, C. A., Weber, O. L., Dalla Villa, R., Vecchiato, A. B., & Pinto, A. A. (2016). Environmental behavior of chlorpyrifos and endosulfan in tropical soil in central Brazil. *Journal of agricultural and food chemistry*, 64(20), 3942-3948.

[66] Wang, P., Yin, Y., Guo, Y., & Wang, C. (2015). Removal of chlorpyrifos from wastewater by wheat straw-derived biochar synthesized through the oxygen-limited method. *RSC advances*, 5(89), 72572-72578.

[67] Broznić, D., & Milin, Č. (2012). Effects of temperature on sorption-desorption processes of imidacloprid in soils of Croatian coastal regions. *Journal of Environmental Science and Health*, Part B, 47(8), 779-794.